# Proteomic analysis of desmosomes reveals novel components required for epidermal integrity

Kwabena A. Badu-Nkansah and Terry Lechler*
Department of Dermatology and Department of Cell Biology, Duke University, Durham, NC 27710

**ABSTRACT** **Desmosomes are cell–cell adhesions necessary for the maintenance of tissue integrity in the skin and heart. While the core components of desmosomes have been identified, peripheral components that modulate canonical or noncanonical desmosome functions still remain largely unexplored. Here we used targeted proximity labeling approaches to further elaborate the desmosome proteome in epidermal keratinocytes. Quantitative mass spectrometry analysis identified all core desmosomal proteins while uncovering a diverse array of new constituents with broad molecular functions. By individually targeting the inner and outer dense plaques, we defined proteins enriched within these subcompartments. We validated a number of these novel desmosome-associated proteins and find that many are membrane proximal proteins that show a dependence on functional desmosomes for their cortical localization. We further explored the mechanism of localization and function of two novel desmosome-associated adaptor proteins enriched in the desmosome proteome, Crk and Crk-like (CrkL). These proteins interacted with Dsg1 and rely on Dsg1 and desmoplakin for robust cortical localization. Epidermal deletion of both Crk and CrkL resulted in perinatal lethality with defects in desmosome morphology and keratin organization, thus demonstrating the utility of this dataset in identifying novel proteins required for desmosome-dependent epidermal integrity.**

**Monitoring Editor**
Denise Montell
University of California, Santa Barbara

Received: Sep 23, 2019
Revised: Feb 21, 2020
Accepted: Mar 26, 2020

## INTRODUCTION

Desmosomes are cell–cell adhesion complexes essential for establishing the mechanical integrity of organs (Garrod and Chidgey, 2008; Kowalczyk and Green, 2013). They are most abundant in tissues that are regularly subjected to mechanical stress such as the epidermis and cardiac muscle (Green and Simpson, 2007; Patel and Green, 2014). Ultrastructurally, desmosomes are highly organized protein complexes with electron-dense plaques whose structural features can be regionalized into nanometer-scale subcompartments (He *et al.*, 2003). The transmembrane core extends across the interface between two cells and contains the extracellular domains of desmosome cadherins, desmocollins, and desmogleins, that form stable calcium-dependent *trans* dimers with cognate cadherins from neighboring cells. Immediately below the plasma membrane is the outer dense plaque region (ODP), where the cytoplasmic domains of these receptors interact with armadillo-domain containing proteins, plakophillins 1–4 (Pkp1,2,3,4) and plakoglobin, which are necessary for efficient formation, clustering, and segregation of desmosome plaques (Kowalczyk *et al.*, 1997, 1999; Hatzfeld, 2007). Further inward is the inner dense plaque (IDP) where desmosome attachment to intermediate filaments (IFs) is facilitated by the core desmosome protein desmoplakin. Desmoplakin is composed of globular head and tail domains connected by coiled-coils that direct formation of parallel homodimers (Green *et al.*, 1990). In mature desmosome plaques, the amino terminus of desmoplakin associates with plakoglobin and PKPs in the ODP, while the carboxy-terminus

This article was published online ahead of print in MBoC in Press (http://www.molbiolcell.org/cgi/doi/10.1091/mbc.E19-09-0542) on April 2, 2020.

*Address correspondence to: Terry Lechler (terry.lechler@duke.edu).

Abbreviations used: BSA, bovine serum albumin; CrkL, Crk-like; DTT, dithiothreitol; ExoC4, Exocyst complex component 4; GEPH, Gephyrin; GST, glutathione-S-transferase; IDP, inner dense plaque; IF, intermediate filament; JCAD, Junctional protein associated with coronary artery disease; LPP, Lipoma-preferred partner; ODP, outer dense plaque; PBS, phosphate-buffered saline; Pdlim5, PDZ and LIM domain protein 5; Pkp, plakophillin; PP1a, protein phosphatase 1; PTPN13, Fas-associated protein-tyrosine phosphatase 1; SH2, Src Homology 2; SH3, Src Homology 3; Shp2, Tyrosine-protein phosphatase nonreceptor type 11; Shrm2, Shroom 2; TEM, transmission electron microscopy; TUFT, glycoprotein Tuftelin.

anchors cortical IFs in the IDP. Therefore, desmoplakin represents a molecular bridge that couples desmosomes to IFs (Green *et al.*, 1992; Bornslaeger *et al.*, 1996; Kowalczyk *et al.*, 1997). These core components represent the canonical functional unit of desmosomes necessary for cell–cell adhesion and tethering of IFs to the cell cortex. However, while traditional biochemical fractionation methods (Skerrow and Matoltsy, 1974; Franke *et al.*, 1981; Mueller and Franke, 1983; Cowin *et al.*, 1986; Heid *et al.*, 1994), cell reconstitution assays (Kowalczyk *et al.*, 1997; Bornslaeger *et al.*, 2001), and genetic models (Allen *et al.*, 1996; Bierkamp *et al.*, 1996; Ruiz *et al.*, 1996; McGrath *et al.*, 1997; Vasioukhin *et al.*, 2001; Samuelov *et al.*, 2013) were fundamental for functionally establishing this molecular core, other studies have identified additional components that either regulate desmosome adhesion/turnover or mediate noncanonical biological functions at desmosomes. For example, in addition to being stable tethers to IFs, unexpected roles for desmosomes in microtubule (Lechler and Fuchs, 2007; Sumigray *et al.*, 2011, 2012) and actin cytoskeleton (Nekrasova *et al.*, 2018) organization have been documented. It is possible that many of these novel components were not previously identified in early fractionation experiments because they are either peripheral, transient, or biochemically labile components that rapidly dissociate upon cell lysis. Therefore, proximity-dependent approaches capable of capturing both stable and transiently localized proteins are necessary to efficiently expand the desmosome proteome.

With the goal of building a complete parts list of desmosomes, we turned to proximity proteomic analysis of desmoplakin's interactome in keratinocytes. Using label-free quantitative mass spectrometry-based analysis, we identified desmosomal proteins enriched within ODP and IDP regions. We validated the localization of novel desmosome-associated proteins and used mouse genetics to define functional roles for two such proteins, Crk and Crk-like (CrkL). Together, proximity-dependent biotinylation combined with label-free quantitative proteomics broadened the compositional landscape of desmosomes, and provided novel insights into biological roles of desmosomes that are essential for the maintenance of epidermal integrity.

## RESULTS

### BioID strategy for targeting desmosome subdomains

To target desmosome-associated proteins, we turned to BioID, a technique that enables local protein biotinylation by mutant variants of the bacterial biotin ligase, BirA (Roux *et al.*, 2012). During maturation, desmosomes become dense, highly insoluble protein structures (Pasdar and Nelson, 1988a,b). While these properties have facilitated purification of core desmosomal proteins, the required extraction conditions are unsuitable for isolating peripheral and/or transiently associated components. BioID circumvents this problem by allowing us to biotinylate proteins localized at desmosomes, thereby making them accessible for purification under harsh conditions and as they transit the soluble fraction. The cytoplasmic face of desmosomes contains two ultrastructurally resolvable units, the IDPs and ODPs (Stahley *et al.*, 2016). To target each of these regions, we constructed fusions of the mutant biotin ligase, $BirA^{R118G}$ (hereafter called BirA) to truncated versions of the core desmosome protein, desmoplakin, which spans these regions. We localized BirA to the outer dense plaque by fusing it to the desmoplakin head domain truncated at $584^{a.a}$ ($Dsp^{N}$-BirA), and to the inner dense plaque region by fusing it to desmoplakin truncated at its coiled-coil domain at $1484^{a.a}$ ($Dsp^{CC}$-BirA) (Figure 1A) (North *et al.*, 1999). We infected primary mouse keratinocyte cells with lentiviral vectors that enabled stable, doxycycline-inducible expression of each construct and, in addition, cytoplasmic-BirA (Cyto-BirA) as a negative control (Figure 1A; Supplemental Figure S1A). These fusion proteins, tagged with HA, stably localized to cortical puncta at cell–cell interfaces (Figure 1B). In calcium shift assays, desmosomes in Dsp–BirA expressing cells rapidly organized at rates and size distributions similar to control cells (Supplemental Figure S1B). Additionally, mature desmosomes in Dsp-BirA expressing cells maintained functional attachments to keratin fibers (Supplemental Figure 1C). Incorporation of biotin was assayed through staining with fluorophore-conjugated streptavidin, revealing close colocalization of biotin signal with endogenous desmoplakin (Figure 1C). Line-scan analysis revealed a clear correlation of the biotin signal with endogenous desmosomes and minimal correlation with adherens junction and tight junction markers, E-cadherin and occludin, respectively (Figure 1C and Supplemental Figure S1D). Under conditions where we expressed equivalent levels of BirA fusions, we saw robust biotinylation by Western blot analysis (Figure 1D). Compared with cytoplasmic controls, we observed more complex banding patterns in cells expressing either Dsp-BirA fusions. Interestingly, we also observed distinct band patterns between $Dsp^{N}$-BirA and $Dsp^{CC}$–BirA expressing keratinocytes, suggesting differential protein interactomes. Initial validation of streptavidin precipitates by Western blot analysis of Dsp-BioID lysates revealed specific enrichment of representative core desmosome proteins from each subcompartment, with minimal enrichment for adherens junction (E-cadherin) and tight junction (occludin) receptors (Figure 1E). Collectively, these results demonstrate desmosome-BioID as a reliable approach for robust labeling and specific purification of desmosome-associated proteins.

### Quantitative mass spectrometry analysis of desmosome-associated proteins

To identify novel desmosome-associated components, we performed label-free quantitative mass spectrometry analysis on triplicate samples of biotinylated proteins purified from $Dsp^{N}$-BirA, $Dsp^{CC}$-BirA, and Cyto–BirA expressing keratinocytes (Figure 2A). We identified hits as significantly enriched at desmosomes if they passed three constraints: 1) a cutoff of twofold average intensity over Cyto-BirA, 2) a protein teller probability greater than 0.8, and 3) a $p$ value of enrichment less than 0.01 calculated by Student's $t$ test analysis when comparing abundance values of $Dsp^{N}$-BirA or $Dsp^{CC}$-BirA hits to Cyto-BirA controls. By this criteria, we identified 628 proteins enriched in $Dsp^{N}$-BirA and 387 in $Dsp^{CC}$-BirA. Of these proteins, 383 were enriched in both samples.

We plotted the intensities of significantly enriched hits for each fusion protein and observed extensive coverage of known core desmosome components (Supplemental Figure S2, A and B). However, our list was not exhaustive, as some previously established desmosome-associated proteins, such as Perp and ninein, were not recovered (Ihrie *et al.*, 2005; Lechler and Fuchs, 2007). In addition to core desmosome components, Desmosome-BioID identified a surprisingly diverse array of proteins from a variety of functional categories (Figure 2, B and C). The most abundant group of hits contained many expected cell junction components, keratins, cortical actin, microtubule, and intermediate filament regulators as well as proteins from unexpected families such as protein kinases, protein phosphatases, and RNA binding proteins; suggesting that the desmosome protein network contains components that link desmosomes to yet unidentified molecular functions (Figure 2C). Additionally, the analysis identified putative regulators of desmosome stability, such as a palmitoyltransferase and thioesterase, which are excellent candidates to mediate the palmitoylation of desmosomal

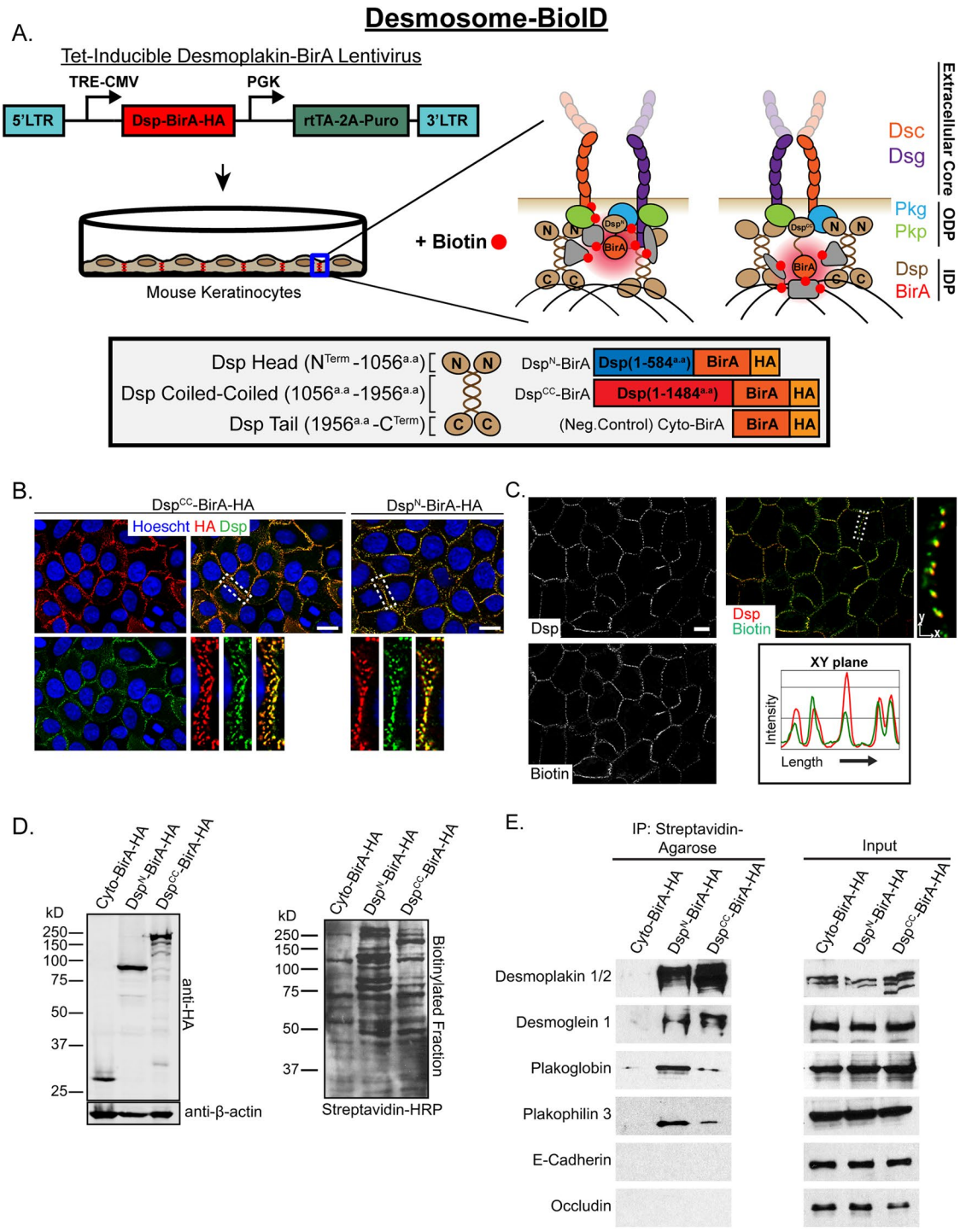


FIGURE 1: Development of desmosome-BioID in keratinocytes. (A) Schematic of doxycyline-inducible BioID approach for targeting desmosomes. BirA, biotin ligase; TRE-CMV, tet-response element promoter; LTR, Long terminal repeat; PGK, 3-phosphoglycerate kinase promoter; rtTA-2A-Puro, reverse tetracycline-controlled transactivator-2A peptide-Puromycin fusion protein; Dsp, desmoplakin; Dsc, desmocollins; Dsg, desmogleins; Pkg, plakoglobin. (B) Validation of Dsp-BirA constructs in mouse keratinocytes immunolabeled for HA-tagged-BirA and Dsp. HA, Hemagglutinin fusion tag; Scale bar, 5 μm. (C) Immunofluorescent labeling of $Dsp^{CC}$-BirA expressing keratinocytes after overnight incubation in $Ca^{2+}$ and exogenous biotin (50 μM). Scale bar, 5μm. Note that the anti-desmoplakin antibody used is to the C-terminus of the protein and does not bind to the BirA fusion proteins. (D) Western blot analysis displays construct expression and biotinylated fraction in biotin-fed, $Ca^{2+}$ induced Dsp-BirA keratinocyte lysates. Membranes were probed with anti-HA and streptavidin-HRP in order to identify Dsp-BirA expression and biotinylation spectrum, respectively. (E) Western blot analysis of junctional components after enrichment of biotinylated fractions from Dsp-BirA lysates. This is representative of three independent experiments.

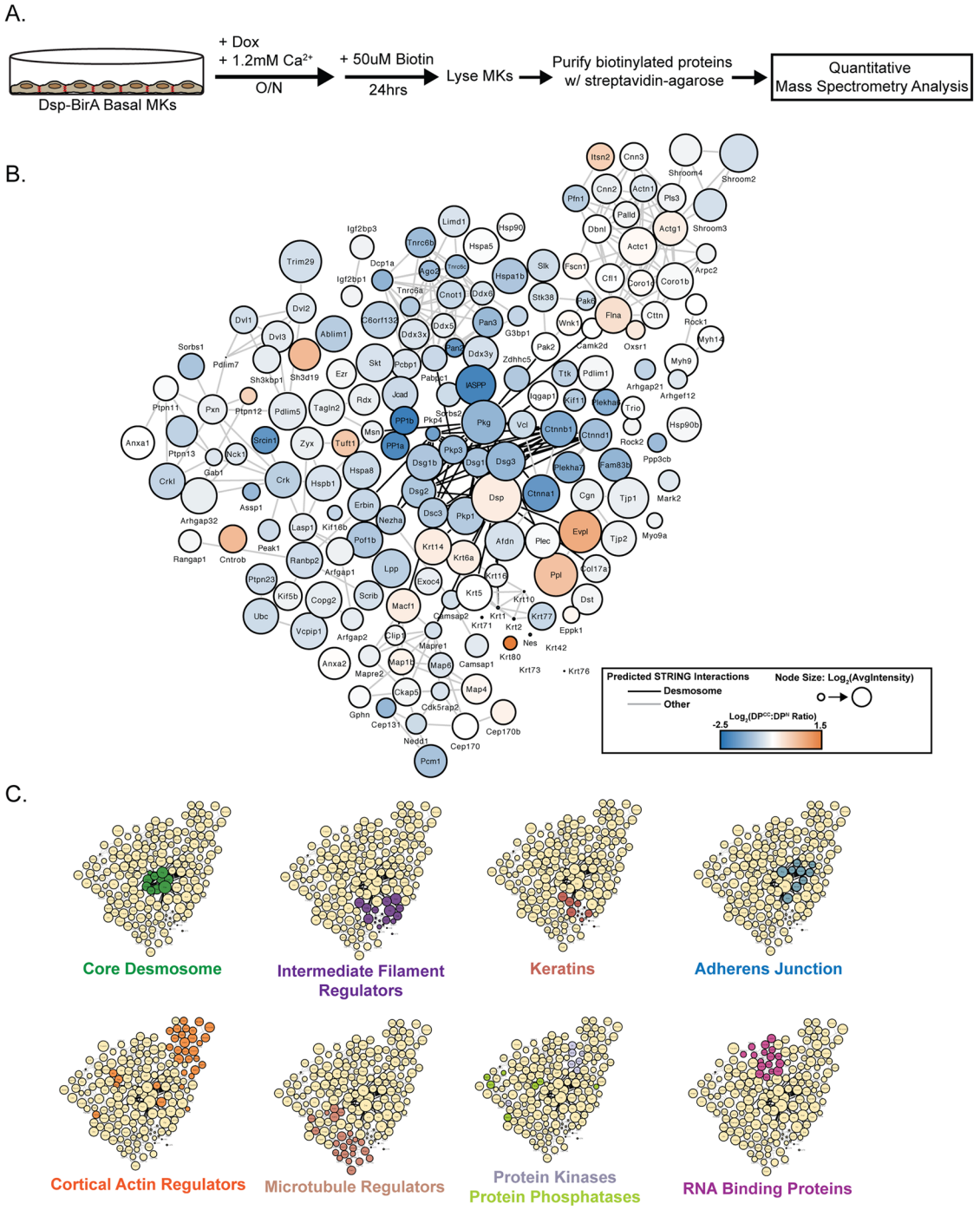


FIGURE 2: Network graph of the desmosome proteome. (A) Outline of desmosome-BioID protocol for proteomic evaluation of desmosomes in keratinocytes. (B) String diagram of top hits from desmosome BioID analyses. Node titles, sizes, and colors represent gene names; total abundances; and $Dsp^{CC}$ vs. $Dsp^{N}$ abundance ratios, respectively; edge connections indicate protein interactions identified by STRING; edge color highlights predicted interactions with core desmosome components. (C) Network topologies of desmosome BioID hits from select protein families.

proteins (Roberts *et al.*, 2014, 2016). To categorize these links, we utilized GO term analysis to identify major biological processes associated with Desmosome-BioID hits. Interestingly, significant categories were not limited to regulators of IFs but also included a number of both microtubule and F-actin interacting proteins, which is consistent with recent work demonstrating that desmosomes can integrate with both cytoskeletal networks (Sumigray *et al.*, 2011, 2012; Godsel *et al.*, 2010; Nekrasova *et al.*, 2018). There was also an enrichment of noncanonical processes such as receptor-mediated endocytosis, cell migration, mRNA transport, and cytoplasmic translation. Lastly, GO term analysis also revealed surprising associations with mRNA:miRNA-binding proteins, an observation previously seen at zonula adherens (Kourtidis *et al.*, 2017), further highlighting that desmosomes may share ancillary molecular functions with adherens junctions in addition to their traditional roles in stabilizing cell–cell attachment and cortical cytoskeleton organization.

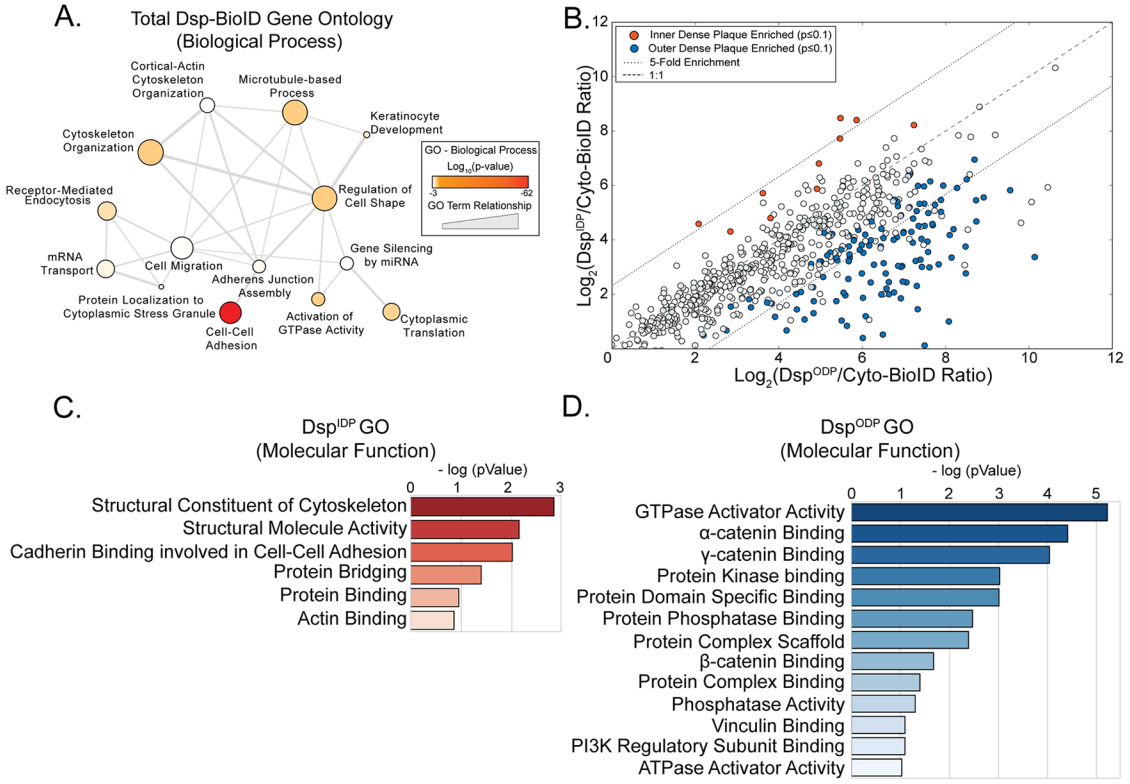


**FIGURE 3:** Characterization and quantitative proteomic analysis of desmosome-BioID. (A) Revigo plot highlighting functional categorization of biological processes enriched by desmosome BioID. Node size represents relative number of proteins while edge width indicates degree of similarity between connecting GO term nodes. (B) Cross-correlation plot compares statistical fold enrichment of protein hits from $Dsp^{IDP}$ vs. $Dsp^{ODP}$ analyses. Each point represents a protein with an associated *p* value indicating enrichment in either $Dsp^{IDP}$ or $Dsp^{ODP}$ conditions, or neither. (C) GO term graph of molecular functions for proteins enriched in $Dsp^{IDP}$. (D) GO term graph of molecular functions for proteins enriched in $Dsp^{ODP}$.

Cross-correlation analysis of $Dsp^{N}$-BirA versus $Dsp^{CC}$-BirA hits revealed substantial overlap and positive correlation between both proteomes, demonstrating that many desmosome-associated proteins were biotinylated in both conditions (Figure 3B). However, we observed a number of proteins that were significantly enriched in one compartment versus the other (Figure 3B and Supplemental Table S1, A and B). Protein hits that were more highly enriched by $Dsp^{CC}$-BirA ($Dsp^{IDP}$) largely included cytoskeletal regulators, confirming previous studies and establishing the IDP as a region where desmosome-cytoskeleton interaction is abundant (Figure 3C; Supplemental Figure 2C). In addition to a clear enrichment of known ODP proteins in the $Dsp^{N}$-BirA ($Dsp^{ODP}$) dataset (including plakophilins, plakoglobin, and desmosomal cadherins), proteins highly enriched in $Dsp^{N}$-BirA were more diverse in molecular functions and included a number of signal transduction regulators such as protein phosphatases and signal adaptor proteins (Figure 3D; Supplemental Figure S2C). This suggests that the proteins enriched in $Dsp^{N}$ versus $Dsp^{CC}$, illustrated in Supplemental Figure. 2C, may represent proteins that are specifically concentrated within each desmosome subcompartment. In particular, these data highlight the ODP as a hub in desmosomes for molecular signaling.

## Desmosomes are essential for cortical localization of novel junctional components

In addition to known desmosome constituents, Dsp-BioID analysis revealed a substantial number of novel desmosome-associated proteins. Intriguingly, we observed that many of these putative components were also identified in previous BioID analyses of adherens junctions (Guo *et al.*, 2014; Van Itallie *et al.*, 2014), tight junctions (Van Itallie *et al.*, 2013), or both. Comparative analysis of similar proximity proteomic studies on adherens junctions and tight junctions reveals significant compositional overlap with the desmosome proteome (Supplemental Figure S3). Since many of these proteins have not been previously shown to localize to desmosomes, we speculated that they may exhibit novel cortical localization in cells with high concentrations of desmosomes, such as keratinocytes. Therefore, we examined the subcellular localization of highly abundant hits using immunofluorescence analysis or fluorescent-protein tagging in calcium-treated mouse keratinocytes. We chose proteins with uncharacterized roles in the epidermis as well as those with known roles but with unspecified localization patterns. Accordingly, immunofluorescence analysis revealed robust cortical localization of Junctional protein associated with coronary artery disease (JCAD), Shroom 2 (Shrm2), PDZ and LIM domain protein 5 (Pdlim5), Lipoma-preferred partner (LPP), Fas-associated protein-tyrosine phosphatase 1 (PTPN13), Tyrosine-protein phosphatase nonreceptor type 11 (Shp2), protein phosphatase 1 (PP1a), the glycoprotein Tuftelin (TUFT), Gephyrin (GEPH), and Exocyst complex component 4 (ExoC4) (Figure 4, A–J). While all of these proteins exhibited varying levels of desmosome colocalization, we observed some unexpected trends. PP1a, PTPN13, and TUFT exhibited high levels of colocalization with desmosomes (>0.6) by Pearson's correlation analysis; ExoC4, GEPH, JCAD, Pdlim5, Shp2, and Shrm2 exhibited mild colocalization (0.3–0.6); and LPP exhibited low colocalization (<0.3).

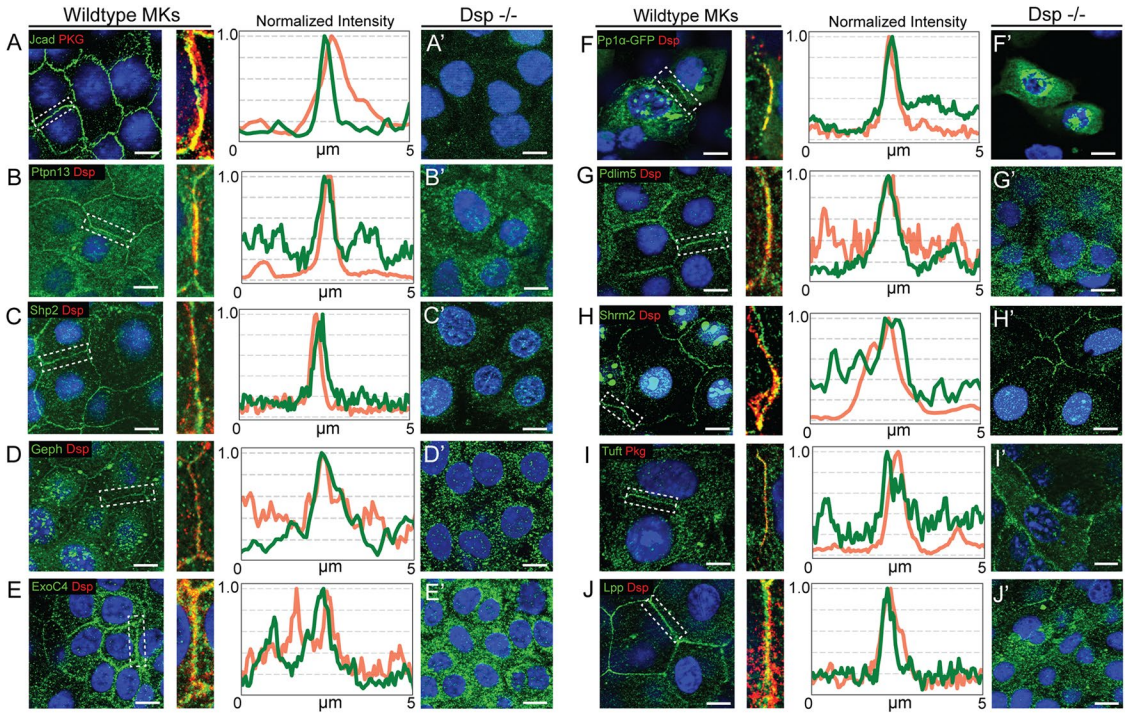


**FIGURE 4:** Validation of select desmosome BioID protein targets identify novel desmosome-associated proteins. Wild-type (A–J) and Dsp –/– (A′–J′) keratinocytes were fixed and costained for desmosomes (red) and candidate proteins, either endogenous or GFP tagged, as indicated. Line scan analyses across desmosomes, depicted in the inset, were used to profile relative enrichment of selected proteins near desmosomes verses the cytoplasm. Corresponding colocalization analyses of these hits are shown in Table 1 which also lists the protein names associated with each gene. Scale bars, 5 μm.

Surprisingly, in spite of their respective levels of desmosome colocalization, we observed that cortical localization of ExoC4, GEPH, JCAD, Pdlim5, and Shp2 was lost in Dsp-null keratinocytes, whereas cortical localization of Shroom2, TUFT, and LPP was independent of desmoplakin (Figure 4, A′–J′). These results are summarized in Table 1. To test whether this was specific to desmosomes, we performed immunofluorescent analysis on p120 catenin-null mouse keratinocytes in which AJs are disrupted (Xiao *et al.*, 2003b; Perez-Moreno *et al.*, 2006). Unlike in Dsp null mouse keratinocytes, in all cases cortical localization was maintained upon loss of p120-catenin (Supplemental Figure S4, A–J). These observations suggest that desmosomes may have uniquely broad influences on cortical protein composition in keratinocytes. Thus, desmosomes may play roles in organizing the cell cortex composition in keratinocytes that are not fully dependent on stable associations with target proteins.

### Functional validation of Crk/CrkL as desmosomal regulators

While validating novel desmosome components identified by Dsp-BioID, we observed an abundance of soluble adapter proteins important for signal transduction. To profile this correlation, we turned to SMART analysis which verified that Src Homology 2 (SH2) and Src Homology 3 (SH3) domains were among the most significantly enriched protein domains of the Dsp-BioID proteome (Figure 5A). We compiled a list of SH3 domain-containing desmosome-associated proteins and noticed many proteins essential for organizing cortical protein complexes at adherens junctions (Fredriksson-Lidman *et al.*, 2017) and focal adhesions (Thomas *et al.*, 1998) (Supplemental Table S2). We focused on Crk and CrkL, paralogous adaptor proteins each composed of one SH2 and two SH3 domains (Figure 5B). Crk and CrkL have been shown to be important mediators of membrane-associated protein complex signaling (Lamorte *et al.*, 2002; Iwahara *et al.*, 2004; Fukuyama *et al.*, 2005) and to regulate clustering of neuromuscular synapses (Hallock *et al.*, 2016), functions that could be relevant in the context of desmosomes. Crk and CrkL were identified in both Dsp-BirA proteomes, with both ~4 times more concentrated in $Dsp^{N}$-BirA over $Dsp^{CC}$-BirA lysates (Figure 5B). Immunofluorescence analysis of endogenous CrkL in mouse keratinocytes revealed punctate cortical localization and robust colocalization with endogenous desmoplakin Figure 5C. Colocalization analyses for CrkL revealed a Pearson coefficient of 0.56 with desmoplakin, as opposed to 0.20 with β-catenin (Figure 5D), demonstrating an enrichment at desmosomes over other adhesions. A similar localization was seen with a Crk-GFP fusion protein, suggesting that both proteins may have redundant functions at desmosomes (Figure 5E). While CrkL pools were largely cytoplasmic in keratinocytes grown in low $Ca^{2+}$, after $Ca^{2+}$ induction we observed robust desmosome recruitment of CrkL 3 h after accumulation of cortical desmoplakin (Figure 5F). In Dsp-null keratinoyctes, cortical localization of CrkL was lost (Figure 5C). However, desmosome localization was unaltered in keratin type II null keratinocytes which lack all keratin filaments, suggesting that desmosome localization of CrkL occurs independently of keratin attachment (Figure 5C). Lastly, cortical loss appeared to be specifically sensitive to disruption of desmosome adhesions, as cortical levels of CrkL were similar between control and p120-catenin null keratinocytes where adherens junction complexes are largely reduced (Figure 5C) (Xiao *et al.*, 2003a; Perez-Moreno *et al.*, 2006). These results indicate that cortical recruitment and stabilization of Crk and CrkL in keratinocytes specifically require assembly of mature desmosomes.

| Uniprot ID | Protein name | $Dsp^{N}$BioID* | $Dsp^{CC}$BioID* | Colocalization** | Cortical localization in Dsp-null cells |
|---|---|---|---|---|---|
| EXOC4 | Exocyst complex component Sec8 | 77 | 67 | 0.39 | N |
| GEPH | Gephryin | 32 | 32 | 0.44 | N |
| JCAD | Junctional protein associated with coronary artery disease | 67 | 32 | 0.44 | N |
| LPP | Lipoma-preferred partner homolog | 149 | 81 | 0.27 | Y |
| PDLI5 | PDZ and LIM domain protein 5 | 90 | 70 | 0.45 | N |
| PP1A | Protein phosphatase PP1-a | 1125 | 387 | 0.85 | N |
| PTN11 | Tyrosine-protein phosphatase nonreceptor type 11 | 171 | 224 | 0.43 | N |
| PTN13 | Tyrosine-protein phosphatase nonreceptor type 13 | 61 | 37 | 0.66 | N |
| SHRM2 | Shroom 2 | 75 | 46 | 0.48 | Y |
| TUFT | Tuftelin | 12 | 41 | 0.66 | Y |

*Fold change enrichment over Cyto-BirA.
**Pearson correlation coefficient values.

**TABLE 1:** Validation of abundant desmosome-BioID hits.

To understand interactions that may promote Crk/CrkL recruitment to the cell cortex, we performed pull-down analysis using recombinant, glutathione-S-transferase (GST)-tagged constructs of either full-length Crk or Crk containing only N-terminal SH2 ($Crk^{SH2}$) or both SH3 domains($Crk^{SH3N/C}$). We found that full-length Crk and $Crk^{SH3N/C}$ each efficiently pulled down Dsg1 from lysates, while the SH2 domain did not (Figure 5G). To gain further evidence for the requirements of this interaction, we examined cortical accumulation of CrkL in human keratinocytes using two approaches: 1) comparison of CrkL localization between HACAT cells, which express Dsg1, to SCC12 cells, a carcinoma line with limited Dsg1 expression (Supplemental Figure S5A) (Denning *et al.*, 1998); and 2) siRNA-mediated knockdown of Dsg1 (Supp. Fig S5C). Consistent with Dsg1 promoting cortical localization of CrkL, we observed a decrease of desmosome localization of Crkl both in SCC12 cells (Supplemental Figure S5B) and in Dsg1 KD HACAT cells (Supplemental Figure S5D). Western blot analysis validated the siRNA knockdown efficiency (Supplemental Figure S5C).

Interestingly, Crkl's enrichment at the cortex increased upon tyrosine phosphatase inhibition by orthovanadate treatment (Supplemental Figure 5, E and F), suggesting a role for the SH2 domain in desmosomal localization as well. Thus, Crk/Crkl may have multiple interactions with desmosomal proteins that are regulated by signaling pathways.

To determine the physiological roles of Crk and CrkL in vivo, we obtained Crk and CrkL floxed mice (Park and Curran, 2008) and mated them to Keratin 14-Cre mice (Vasioukhin *et al.*, 1999), allowing for efficient recombination in the epidermis and subsequent loss of Crk/CrkL (Figure 6, A and B). Homozygous loss of either Crk or CrkL alone did not result in any gross observable phenotype. However, homozygous loss of both Crk and CrkL together (Crk/$L^{dKO}$) resulted in neonatal lethality with greater than 50% penetrance. Mutant neonatal pups displayed a compromised epidermis indicative of a significant loss of intercellular cohesion (Figure 6C). These observations are in agreement with previous studies showing that Crk and CrkL have overlapping functions in vivo (Park and Curran, 2008).

Histologic examination of newborn epidermis in Crk/$L^{dKO}$ mice revealed small intercellular separations dispersed throughout the mutant epidermis, consistent with phenotypes associated with mild desmosome disruption (Figure 6, D and E). Transmission electron microscopy (TEM) of Crk/$L^{dKO}$ skin revealed frequent cell–cell separations throughout the epidermis that were particularly prevalent among differentiated keratinocytes in spinous and granular layers (Figure 6, D and E). Evaluation of EM micrographs revealed that desmosome morphologies were significantly disrupted in Crk/$L^{dKO}$ skin (Figure 6F). Most frequently we noted lack of density in the ODP and particularly in desmosomes adjacent to cell-cell separations (Figure 6, E and F). These morphological defects were not associated with increased proliferation or apoptosis (unpublished data), nor were they accompanied by changes in the expression patterns of differentiation markers including keratin 5/14 (basal cell marker), keratin 10 (spinous and granular cell marker), and loricrin (granular cell marker) (Figure 6H; Supplemental Figure S6A).

We next analyzed the localization of desmosomal proteins in Crk/$L^{dKO}$ epidermis by immunofluorescence. While desmoplakin and desmoglein 1 localization appeared largely normal, we observed a decrease in cortical plakoglobin levels scattered throughout mutant epidermis (Figure 6G). Line scan analyses validated a defect in cortical enrichment of plakoglobin in the mutant skin (Figure 6G). In contrast, no defects were noted in either E-cadherin or cortical F-actin localization or levels (Supplemental Figure S6B). Interestingly, while keratin organization within the basal layer appeared largely normal, keratin 10 in subrabasal layers was often collapsed around the nucleus (Figure 6H, inset). These data demonstrate a physiological role for Crk/Crkl in epidermal integrity and in desmosome morphology. Further analysis will be required to determine whether Crk/Crkl has additional roles outside of the desmosome in the epidermis. Together, this demonstrates a proof of principle that Dsp-BioID analysis increased not only the complexity of the desmosome proteome but also revealed functional regulators of keratinocyte structure and epidermal integrity.

## DISCUSSION

In this study, we used BioID to evaluate the desmosome proteome in epidermal keratinocytes and identify novel desmosome-associated proteins. Newly identified components contained a surprisingly varied array of molecular functions that only partly overlapped with known molecular roles at desmosomes. Of these were numerous scaffolding proteins that harbor adapter domains seemingly

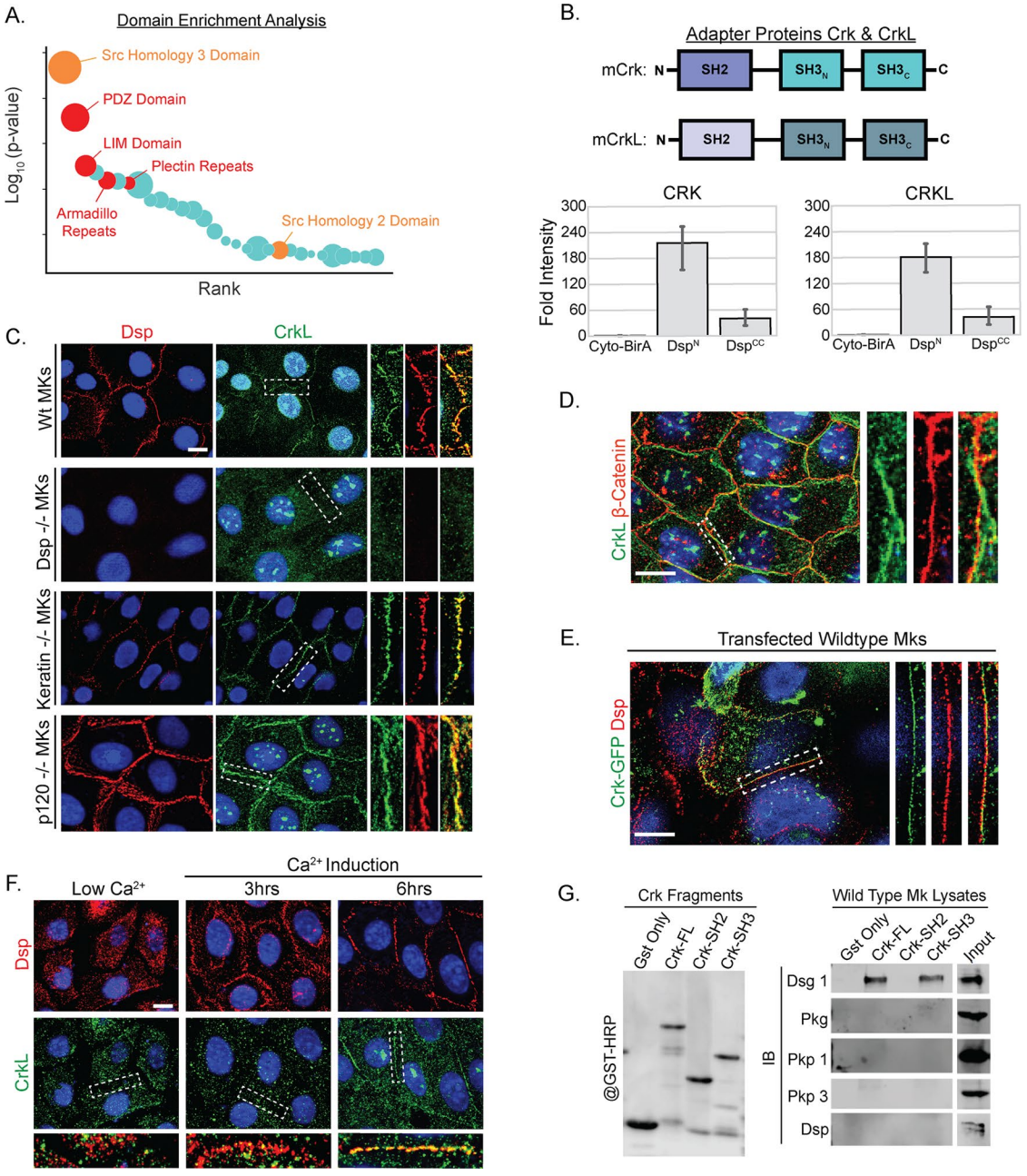


FIGURE 5: Adapter molecules Crk and CrkL are novel desmosome constituents. (A) Domain enrichment analysis of desmosome BioID using SMART. (B) Schematic representation of domains in Crk and CrkL and graphs displaying fold enrichment of Crk and CrkL in Dsp-BirA proteomes over Cyto-BirA. (C) Desmosome (Dsp, red) and CrkL (green) staining in Wt, Dsp –/–, Keratin –/–, and p120-catenin –/– keratinocytes after 24hr $Ca^{2+}$ incubation. (D) Staining for Crkl (green) and β-catenin (red) in cultured keratinocytes after 24h $Ca^{2+}$ incubation. (E) Immunofluorescent staining of desmosomes (Dsp, red) and GFP (green) in $Ca^{2+}$ induced mouse keratinocytes transfected with full length Crk-GFP. (F) Time course of localization after calcium-induced desmosome formation. Immunofluorescent staining of desmosomes (Dsp, red) and CrkL (green) in mouse keratinocytes before and after $Ca^{2+}$ induction. (G) Pull-down assays from mouse keratinocyte lysates using recombinant Crk constructs reveal associations between Crk and desmoglein 1. This is representative of two independent replicates.

important for stabilizing protein interactions necessary for downstream signal transduction. We were able to validate the localization of novel desmosome scaffold proteins and additionally used mouse genetics to identify essential functions in epidermal integrity for the adaptor proteins Crk and CrkL.

Proximity proteomics has now been performed for all major cell–cell junction complexes of vertebrates (Van Itallie *et al.*, 2013; Guo *et al.*, 2014). Here we report a surprisingly high degree of compositional overlap with BioID analyses of AJs and TJs. While it is possible that some of this overlap is due to labeling promiscuity of BirA, an intriguing alternative is that this overlap indicates junctional cross-talk driven by direct interactions, compositional sharing, and/or functional proximity between distinct junction complexes. A classic example of compositional sharing between desmosomes

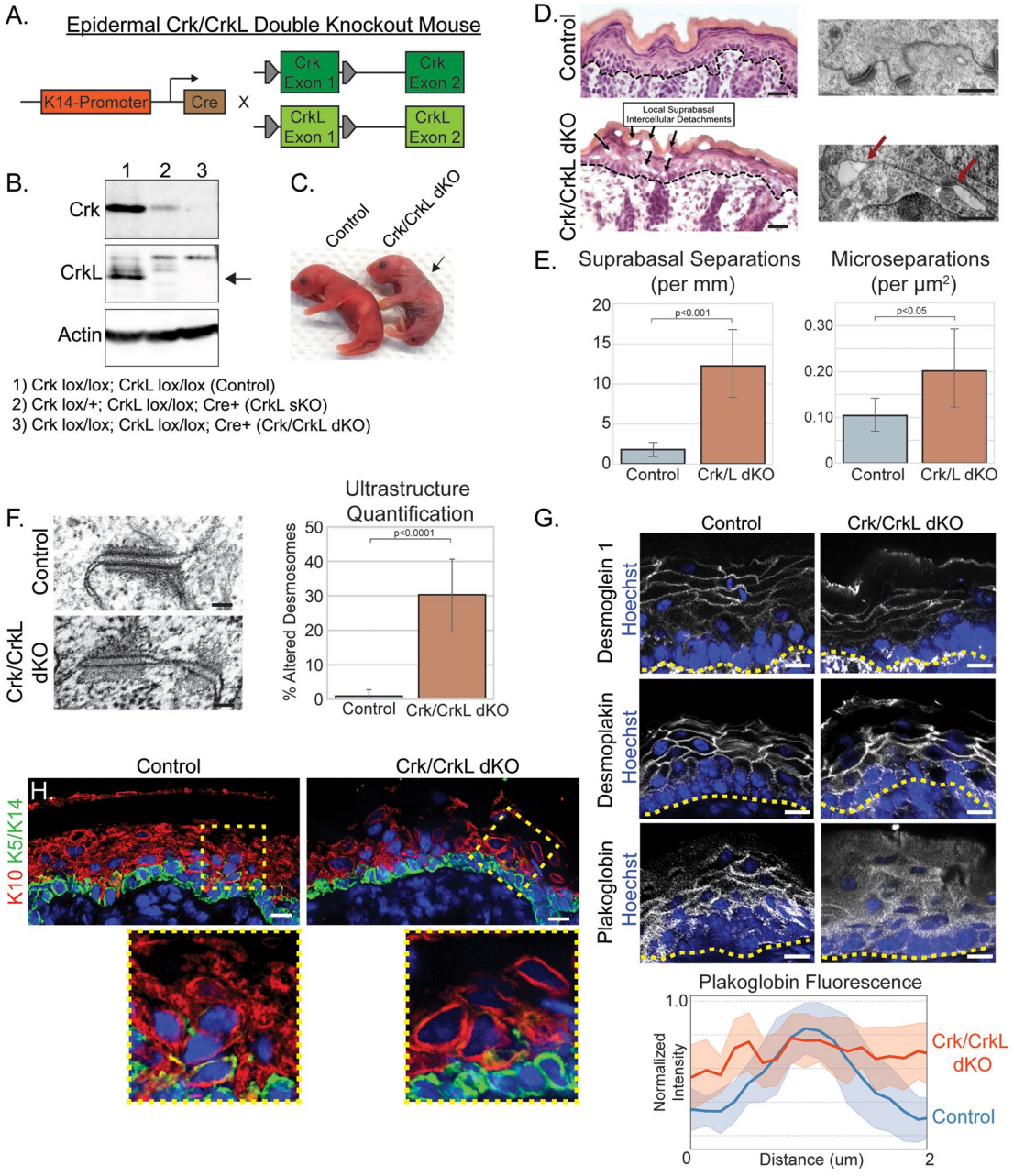


FIGURE 6: Tissue-specific loss of Crk and CrkL results in acantholysis and altered desmosome morphologies in the epidermis. (A) Genetic strategy for epidermal targeting of Crk and CrkL. (B) Western blot analysis of isolated epidermis from control and dKO mice. Arrow points to band representing loss of CrkL protein. (C) Representative images of control and dKO newborn pups. Note compromised patches of epidermal tissues designated by arrow. (D) H&E (left) and transmission electron microscopy (right) images of control and mutant skin. Note intercellular detachments designated by arrows. Scale bars, left, 30 μm; right, 500 nm. (E) Quantitative analysis of intercellular separations from (left) H&E (n=4 mice) and (right) transmission electron microscopy ($n$ = 15 regions, 2 mice). (F) Left: high magnification transmission electron micrographs of control and Crk/CrkL dKO epidermis. Right: quantitation of disrupted desmosome organization in the control and Crk/CrkL dKO skin. Scale bars, 100 nm ($n$ = 15 regions, 2 mice). (G) Top: representative immunofluorescent stains of desmoglein 1, desmoplakin, and plakoglobin in control and mutant epidermis. Dashed line delineates cell membrane area. Scale bars, 20 μm. Bottom: line scan analysis of plakoglobin stains across cell–cell interfaces, Shaded regions represent standard deviation from mean. ($n$ = 20 scans, 3 mice). (H) Representative immunofluorescent stains of differentiation related markers keratin 10 (red) and keratin 5/14 (green) in control and dKO epidermis. Inset: Note the perinuclear accumulation of keratin in suprabasal cells of mutant mice. Scale bars, 20 μm.

and adherens junctions is in vascular endothelial cells that harbor hybrid junctions containing plakoglobin and desmoplakin along with p120-catenin, among other adherens junction proteins (Schmelz *et al.*, 1994; Kowalczyk *et al.*, 1998; Hammerling *et al.*, 2006). The overlap between AJ (performed in simple epithelial cells) and desmosome (performed in keratinoyctes from stratified epidermis)

proteomes may reflect a switch from an AJ-dominant localization often found in simple epithelia to high levels of desmosome-dependent localization in stratified epithelia, where desmosomes are a predominant cell adhesion structure. Such a view is consistent with the conserved molecular architecture of desmosomes and adherens junctions, with paralogous armadillo repeat proteins in each.

An emerging view is that desmosomes integrate many aspects of cell physiology in addition to IF attachment (Kowalczyk and Green, 2013). In this study, Desmosome-BioID analysis hinted that functional desmosomes are permissive for a stable cortical protein environment in keratinocytes. This is particularly pertinent for understanding the differentiated epidermis where desmosomes may provide a means to communicate the status of cell cohesion by integrating cell–cell attachment to the activity of cortical signaling complexes.

We found a large number of both SH2/SH3 adaptor proteins and protein tyrosine phosphatases in our desmosome BioID analysis. This raises a question of the role of desmosomes in regulating and being regulated by phospho-tyrosine signaling, which has not been well studied. SH2/SH3 proteins have also been shown to regulate many cortical complexes including focal adhesions (O'Neill *et al.*, 2000), synapses (Okada *et al.*, 2011), and other cell–cell adhesions (Mandai *et al.*, 1999; Nomme *et al.*, 2011b). Previous reports have identified SH2/SH3 domain-containing proteins in tight junctions and adherens junctions that are essential for maintaining proper junctional structure (McNeil *et al.*, 2006; Nomme *et al.*, 2011a) and junctional stability (Woodcock *et al.*, 2009). It is also possible that these signaling pathways do not directly control adhesion but are downstream of sensors of the adhesion state that respond to loss of epidermal integrity.

We demonstrated a functional role for Crk and CrkL at desmosomes in the epidermis. Notably, Crk and CrkL are required for the clustering of receptors at neuromuscular synapses (Hallock *et al.*, 2016). This function requires their association with Sorbin1/2, adaptor proteins containing SH3 domains, which were also identified in our proteomic analysis of desmosomes. While the detailed mechanism of action of these proteins at either neuromuscular junctions or desmosomes is not yet clear, these data raise the intriguing possibility that Crk/CrkL/Sorbin1/2 may form a modular unit that promotes clustering of membrane complexes and is regulated by signal transduction pathways. Crk and CrkL have also been proposed to promote adherens junction integrity through actin cytoskeleton regulation downstream of Rho GTPases in MDCK cells (Zandy *et al.*, 2007). However, in keratinocytes, CrkL colocalizes more strongly with desmosomes than adherens junctions and requires desmosomal proteins but not adherens junction proteins for its cortical localization. While we did not note a steady state difference in F-actin localization, we cannot rule out that Crk/Crkl may affect this cytoskeletal network. We also report a novel association between Crk/CrkL and Dsg1, therefore providing the first evidence that desmosome complexes may also employ SH2/SH3 domain adaptor proteins for proper molecular functions. A motif scan analysis of core desmosome components reveals variants of putative proline-rich motifs which are possible substrates for SH3 domains. The function of these adapter proteins and how they integrate desmosomes with other aspects of cell physiology require further investigation.

## MATERIALS AND METHODS

### Plasmids

Doxycycline-inducible Dsp-BirA fusion constructs were created by PCR amplifying HA-BirA (Addgene #36047; Roux *et al.*, 2012) and inserting it between Nhe1-Age1 sites in plix402 (Addgene #41394). $Dsp^{N}$ and $Dsp^{CC}$ truncations were PCR amplified from human cDNA (Addgene #32227; Godsel *et al.*, 2005) and inserted into plix402-HA-BirA between Nhe1-BstB1 sites. Gephryn-GFP was a gift from Scott Soderling (Duke University). PP1alpha GFP (Addgene #44224; Trinkle-Mulcahy *et al.*, 2001), Crk-GFP(Addgene #50730), and CrkL cDNA (Addgene #23354; Johannessen *et al.*, 2010) were all obtained from Addgene. Biotinylated nontargeting siRNA (5′GGGAACCGUAUAGAGUCAGUAAAGU3′) and siRNA against human Dsg1 using a previously published targeting sequence(Nekrasova *et al.*, 2018) (5′-CCATTAGAGAGTGGCAATAGGATGA-3′) were synthesized by Integrated DNA Technologies.

### Cell culture

All cell culture studies were performed on mouse and human keratinocytes. All keratinocyte cell lines were grown at 37°C and 7.5% CO2. Mouse keratinocytes were isolated from the backskin of e18.5 embryos by dispase treatment and trypsinization. After several passages on fibroblast feeders, keratinocyte lines were grown in the absence of feeders in low calcium keratinocyte media (3 1 DMEM:F12 [Invitrogen] with insulin (Sigma, 0.5 µg/ml), cholera toxin (ICN Biomedicals, 0.1 nM), transferrin (Sigma, 0.5 µg/ml), hydrocortisone (Calbiochem, 0.4 µg/ml), and T3 (Sigma, 0.2 µM) with 15% fetal bovine serum (Hyclone), which was first chelated with Chelex (Bio-Rad) to remove calcium and afterward supplemented to a final concentration of 0.05 mM with $CaCl_2$). To establish stable Dsp-BirA cell lines, we infected mouse keratinocytes overnight with BirA lentiviral vectors and subsequent selection 2 µg/ml puromycin. Unless otherwise indicated, mouse keratinocytes were cultured in low $Ca^{2+}$ keratinocyte media (0.05 mM) until desmosome induction on which cell media were switched to high $Ca^{2+}$ (1.5 mM) media either through the addition of 2M $CaCl_2$ or by switching media with unchelated keratinocyte media. Keratinocytes were then kept in high $Ca^{2+}$ (1.5 mM) media for indicated timepoints up through 48 h. SCC cells were gifts from the Jennifer Zhang lab (Duke University Medical Center, Department of Dermatology). All DNA transfections were performed using Mirus- LT1 reagent and siRNA transfections were performed using ViroMir Red.

### Mice

All animal work was approved by Duke University's Institutional Animal Care and Use Committee. Mice were genotyped by PCR amplification of mutant alleles and both males and females were analyzed. Mice were maintained in a barrier facility with 12-h light/dark cycles. Mouse strains used in this study were Crk fl/fl and CrkL fl/fl (both gifts from Tom Curran, The Children's Hospital of Philadelphia, C57BL/6J) (Park and Curran, 2008) and Krt14-Cre (a gift from Elaine Fuchs, Rockefeller University, CD1) (Vasioukhin *et al.*, 1999). All control and mutant mice carrying Crk fl/fl, CrkL fl/fl, and Krt14-Cre alleles were mixed strains from C57BL/6J and CD1 parents.

### Immunofluorescence

Cells were fixed in either 100% methanol at –20°C for 3 min or 4% paraformaldehyde for 5 min. Depending on antibody, cells were also pre-extracted in 0.1% Triton at 37°C for 30 s before fixation. All epidermal stains were performed on mouse tissue. Mouse skin tissue was collected from postnatal day 0 pups, mounted on paper towel, embedded in OCT compound (Sakura 4583), and frozen over dry ice. Frozen blocks were stored long term in –80°C before being cut into 8-µm sections on a cryostat and mounted on glass slides. Sections were postfixed in either 100% methanol at –20°C

for 3 min or 4% paraformaldehyde for 7 min before permeabilization in 0.1%Triton and subsequent staining. Cells and tissue were blocked and stained in blocking buffer (5% normal goat serum, 3% normal donkey serum, 0.1% Triton). Endogenous desmosomes were visualized using a desmoplakin monoclonal antibody (Millipore Sigma, MABT1492) that targets desmoplakin's C-termini distal from both Dsp-BirA truncations. Primary antibodies used were CrkL (Santa Cruz, sc-319, sc-365092), Crk (BD Bioscience, 610035), Dsg1 (BD Bioscience, 610273), Desmoplakin (Millipore Sigma, MABT1492), E-Cadherin (Invitrogen, 13-1900), GFP (Abcam, ab13970), HA tag (Roche, 11867423001), JCAD (Santa Cruz, sc-515169), Occludin (Thermo Fisher, 71-1500), Plakoglobin (Santa Cruz, sc-7900; Abcam, ab184919), PTPN13 (Santa Cruz, sc-15356), Shroom2 (GeneTex, GTX100055), Shroom3 (Santa Cruz, sc-376125), Streptavidin-488 (Thermo S11223), and TRITC-Phalloidin (Sigma, P1591). Secondary antibodies used were Donkey Alexa Fluor 488– and 647–conjugated series (Life Technologies/Thermo Fisher) and Donkey Rhodamine Red–conjugated series (Jackson ImmunoResearch). All cell stain analyses were performed three times with each independent replicate quantitation representing at least 40 cells. Line scans for all analyses were collected using Fiji. Fluorescent intensities were measured across 2- to 5-μm lines centered on the plasma membrane over multiple fluorescent channels when necessary. Intensity data were exported from Fiji to Excel and normalized for quantitative analysis. Line graphs were made using Matplotlib and Seaborn libraries in Python v3.6.

### Hematoxylin and eosin stain

Frozen tissue sections were prepared as above. Sections were postfixed in 10% PFA at 4°C for 10 min. Sections were washed and stained in Mayers Hematoxylin (Sigma-Aldrich, MHS32-1L) solution for 10 min, followed by rinsing under running water, five dips into Eosin (Polysciences, 09859), dehydration series into 100% ethanol, xylene clearing, and mounting in Permount mounting media. Tissues were coverslipped and sealed using nail polish. Quantitative analyses of Crk/CrkL mutant tissue were performed blinded on at least five different regions from four independent mouse litters containing both control and mutant pups.

### Transmission Electron Microscopy

Whole backskin was isolated from control and mutant newborn pups and fixed in 4% glutaraldehyde, 1 mM $CaCl_2$, and 0.05 M cacodylic acid (pH 7.4), for 3 h at room temperature and then overnight at 4°C. Samples were washed in 0.1 M sodium cacodylate buffer containing 7.5% sucrose. Samples were postfixed in 1% osmium tetroxide in 0.15 M sodium cacodylate buffer for 1 h and then washed in two changes of 0.11 M veronal acetate buffer for 15 min each. Samples were placed into en bloc stain (0.5% uranyl acetate in veronal acetate buffer) for 1 h, washed in veronal acetate buffer, and then dehydrated in a series of 70, 95, and 100% ethanol. Finally, samples were prepared in 50/50 propylene oxide:Epon resin followed subsequently by two 30-min immersions in 100% Epon resin for embedding. Skin samples were sectioned and imaged with a CM12 transmission electron microscope (Phillips) run at 80 kV with an XR60 camera (Advanced Microscopy Techniques, Woburn, MA). Image acquisition was done using 2Vu software (Advanced Microscopy Techniques). TEM images were visualized using FIJI software. Desmosome morphologies and microseperations were examined in the spinous and granular layers of suprabasal epidermis for all mice. Quantitative analyses of control and mutant epidermis were done for least 15 different regions from two independent mouse litters containing both control and mutant pups.

### Microscopy

Cell stains and tissue sections were imaged on a Zeiss AxioImager Z1 microscope with an Apotome 2 attachment using either Plan-APOCHROMAT 40×/1.3 objective oil objective or Plan-NEOFLUAR 63×/1.4 oil objective, Axiocam 506 mono camera for fluorescent images or AxioCam MRc camera for H&E Stains, and Zen software (Zeiss).

### Immunoblots

Cells were lysed at 4°C in RIPA buffer (50 mM Tris, pH 8, 1% Triton, 150 mM NaCl, 0.5% SDS, 50 mM Triton, 1 mM EDTA) + Protease Inhibitor Cocktail (Roche, 11697498001), sonicated for 15 s, clarified via centrifugation, and stored in –80°C. Lysates were solubilized by mixing 1:1 in loading buffer (10% SDS, 40% glycerol, 3% Bromophenyl Blue, and 10% Beta-Mercaptoethanol). Proteins in lysates with loading buffer were first denatured by boiling for 5 min and cooled on ice for 2 min before being loaded into 10% polyacrylamide gels and run for ~90 min at 125V. Resolved proteins were transferred onto nitrocellulose membranes for 1 h at 100V. Membranes were then blocked with 5% bovine serum albumin (BSA) for an hour before incubation with primary antibody, washed three times in PBST (2.0% Triton in phosphate-buffered saline [PBS]), and then finally incubated with secondary antibodies (Licor, IRDye 680RD Series, CW800 Series). Bands were visualized using a LI-COR Odyssey FC system. Primary antibodies used were Dsg1 (BD Bioscience, 610273), Desmoplakin (Millipore Sigma, MABT1492), E-cadherin (Invitrogen, 13-1900), GST (Bethyl Laboratories, A190-122P), HA tag (Roche, 11867423001), Occludin (Thermo Fisher, 71-1500), Plakoglobin (Santa Cruz, sc-7900), and Streptavidin-HRP (Thermo Fisher, 43-4323).

### Crk-GST isolation and pull downs

Full-length and subdomains of Crk and CrkL cDNA were PCR amplified and cloned upstream of GST between NotI and SalI sites in pGEX-4T1. Recombinant GST fusion proteins were produced in BL21 cells via IPTG induction and isolated from bacterial lysate after sonication in buffer PB (PBS, 1 mM EGTA, 1 mM EDTA, phenylmethylsulfonyl fluoride, 1 mM dithiothreitol [DTT], Protease Inhibitor Cocktail). Bacterial lysates were clarified through centrifugation and supernatant was incubated in glutathione agarose for 1 h at 4°C. Crk–GST-loaded beads were washed twice in PBST (0.1% Tween-20 + 1 mM DTT) and fusion proteins were eluted in elution buffer (50 mM Tris, pH 8.0, 5 mM reduced gluthathione, 1 mM DTT). Samples were dialyzed into PBS overnight and protein concentrations were measured via Bradford assay. Dialyzed samples were flash frozen in liquid nitrogen and stored at –80°C.

Crk-GST pull downs were performed as follows: recombinant full-length and truncated Crk-GST fusions were incubated in clarified lysates from $Ca^{2+}$ induced mouse keratinocytes for 2 h at 4°C. GST-beads were next incubated with Crk-GST mix for at least 3 h. Beads were subsequently washed 3 times in wash buffer, resuspended in loading buffer, and eluted via boiling for 5 min before loading into protein gel for immunoblot analysis. All published GST-pulldowns experiments were repeated at least three times.

### Purification of biotinylated proteins

Mouse keratinocytes stably expressing $Dsp^{N}$-BirA or $Dsp^{CC}$-BirA were maintained and grown in low $Ca^{2+}$ until 70% confluence. Cells were then incubated overnight with high $Ca^{2+}$ (1.5 mM) media containing 2 μg/ml doxycycline to induce Dsp-BirA expression concomitantly with desmosome organization; 100 μM biotin were next added to the media and incubated for 24 h before cell lysis

(see above). Clarified lysates were incubated with Neutravidin beads (Pierce/Thermo, 29200) overnight at 4°C. Beads were washed once with 2% SDS buffer, once with DOC wash buffer (50 mM HEPES, pH 7.3, 0.1% deoxycholate, 1% Triton X-100, 500 mM NaCl, 1 mM EDTA), once with salt buffer (10 mM Tris, pH 8.0, 250 mM LiCl, 1 mM EDTA, 0.5% deoxycholate, 0.5% NP40) and twice with wash buffer (50 mM Tris, pH 7.5, 50 mM NaCl). For immunoblots, beads were resuspended in loading buffer with saturated biotin and for mass spectrometry analysis beads were resuspended in Elution buffer (250 mM Tris, pH 6.8, 4% SDS, 0.57 M Beta-mercaptoethanol, 10% glycerol with saturated biotin). In both cases, bound proteins were eluted via boiling at 95°C for 5 min.

### Mass spectrometry analysis

BirA, Dsp$^{N}$-BirA, and Dsp$^{CC}$-BirA samples were each generated and analyzed in triplicate. Each sample was briefly run through a 4–12% gradient SDS–PAGE gel and subjected to in-gel reduction, alkylation, and tryptic digestion. Samples were isolated from gel, lyophilized, and resolubilized in 80 µl of 2% acetonitrile/1% TFA supplemented with 10 fmol/µl yeast ADH. From each sample, 5 µl was removed to create a QC Pool sample which was run periodically throughout the acquisition period. Quantitative LC/MS/MS was performed on 1 µl of each sample, using a nanoAcquity UPLC system (Waters Corporation) coupled to a Thermo QExactive Plus high-resolution accurate mass tandem mass spectrometer (Thermo) via a nanoelectrospray ionization source. The sample was first trapped on a Symmetry C18 trapping column (5 µl/min at 99.9/0.1 water/acetonitrile), after which analytical separation was performed using a 1.7 µm Acquity BEH130 C18 column (Waters Corporation) with a 90-min linear gradient of 5–40% acetonitrile with 0.1% formic acid at a flow rate of 400 nl/min at 55°C. Data collection on the QExactive Plus mass spectrometer was performed in a data-dependent acquisition mode with a $r = 70{,}000$ (m/z 200) full MS scan from m/z 375–1600 with a target AGC value of $10^6$ ions followed by 10 MS/MS scans at $r = 17{,}500$ (m/z 200) at a target AGC value of $5^4$ ions. A 20-s dynamic exclusion was employed to increase depth of coverage. Following 12 total UPLC-MS/MS analyses, data were imported into Rosetta Elucidator v 4.0 (Rosetta Biosoftware), and analyses were aligned based on the accurate mass and retention time of detected ions using PeakTeller algorithm in Elucidator. Relative peptide abundance was calculated based on area-under-the-curve of the selected ion chromatograms of aligned features across all runs. The MS/MS data were searched against a custom Swissprot database with *Mus musculus* taxonomy (circa 2015) with additional proteins, including yeast ADH1, BSA, *Escherichia coli* BirA, as well as an equal number of reversed-sequence "decoys" to assess false discovery rate determination. Mascot Distiller and Mascot Server (v 2.5, Matrix Sciences) were utilized to perform the database searches. After individual peptide scoring using the PeptideProphet algorithm in Elucidator, the data were annotated at a 1.3% peptide false discovery rate. Compiled data were stored in Excel files containing raw and normalized quantitative values for each peptide/protein, each replicate, quality control scores, statistical analysis comparisons between Dsp$^{CC}$-BirA, Dsp$^{N}$-BirA, and Cyto-BirA. Enriched gene lists were imported into DAVID (https://david.ncifcrf.gov/summary.jsp) and REVIGO (Supek *et al.*, 2011) for GO term enrichment analysis. All corresponding charts/graphs were made using Matplot lib and Seaborn libraries in Python v3.6.

### Network analysis

Enriched protein hits in Dsp$^{CC}$-BirA and Dsp$^{N}$-BirA were determined through statistical comparisons to cytoplasmic-BirA. For both overall desmosome proteome and junctional comparison networks, the top 200 most enriched unique proteins in Dsp$^{CC}$-BirA and Dsp$^{N}$-BirA proteomes were used. Predicted interactions between enriched proteins were determined in STRINGdb (https://string-db.org/). Interaction data, protein symbols with corresponding average intensity readings were imported into Cytoscape v3.4.0 as edges, nodes, and node features, respectively, for network visualization. To incorporate proteomes of adherens junctions and tight junctions data for network visualization, data from separate BioID analyses targeting corresponding junctions were used (Van Itallie *et al.*, 2013, 2014; Guo *et al.*, 2014).

## ACKNOWLEDGMENTS

We thank Tom Curran and Elaine Fuchs for mouse strains and Julie Underwood for care of the mice, as well as all members of the Lechler lab for contributions to the manuscript. This work was supported by an HHMI Gilliam Fellowship (to K.B.) and by National Institutes of Health grants R01-AR055926 and R01-AR067204 (to T.L.).

## REFERENCES

Allen E, Yu QC, Fuchs E (1996). Mice expressing a mutant desmosomal cadherin exhibit abnormalities in desmosomes, proliferation, and epidermal differentiation. J Cell Biol 133, 1367–1382.

Bierkamp C, McLaughlin KJ, Schwarz H, Huber O, Kemler R (1996). Embryonic heart and skin defects in mice lacking plakoglobin. Dev Biol 180, 780–785.

Bornslaeger EA, Corcoran CM, Stappenbeck TS, Green KJ (1996). Breaking the connection: displacement of the desmosomal plaque protein desmoplakin from cell-cell interfaces disrupts anchorage of intermediate filament bundles and alters intercellular junction assembly. J Cell Biol 134, 985–1001.

Bornslaeger EA, Godsel LM, Corcoran CM, Park JK, Hatzfeld M, Kowalczyk AP, Green KJ (2001). Plakophilin 1 interferes with plakoglobin binding to desmoplakin, yet together with plakoglobin promotes clustering of desmosomal plaque complexes at cell-cell borders. J Cell Sci 114, 727–738.

Cowin P, Kapprell HP, Franke WW, Tamkun J, Hynes RO (1986). Plakoglobin - a protein common to different kinds of intercellular adhering junctions. Cell 46, 1063–1073.

Denning MF, Guy SG, Ellerbroek SM, Norvell SM, Kowalczyk AP, Green KJ (1998). The expression of desmoglein isoforms in cultured human keratinocytes is regulated by calcium, serum, and protein kinase C. Exp Cell Res 239, 50–59.

Franke WW, Schmid E, Grund C, Muller H, Engelbrecht I, Moll R, Stadler J, Jarasch ED (1981). Antibodies to high molecular-weight polypeptides of desmosomes - specific localization of a class of junctional proteins in cells and tissues. Differentiation 20, 217–241.

Fredriksson-Lidman K, Van Itallie CM, Tietgens AJ, Anderson JM (2017). Sorbin and SH3 domain-containing protein 2 (SORBS2) is a component of the acto-myosin ring at the apical junctional complex in epithelial cells. PLoS One 12, e0185448.

Fukuyama T, Ogita H, Kawakatsu T, Fukuhara T, Yamada T, Sato T, Shimizu K, Nakamura T, Matsuda M, Takai Y (2005). Involvement of the c-Src-Crk-C3G-Rap1 signaling in the nectin-induced activation of Cdc42 and formation of adherens junctions. J Biol Chem 280, 815–825.

Garrod D, Chidgey M (2008). Desmosome structure, composition and function. Biochim Biophys Acta 1778, 572–587.

Godsel LM, Hsieh SN, Amargo EV, Bass AE, Pascoe-McGillicuddy LT, Huen AC, Thorne ME, Gaudry CA, Park JK, Myung K, *et al.* (2005). Desmoplakin assembly dynamics in four dimensions: multiple phases differentially regulated by intermediate filaments and actin. J Cell Biol 171, 1045–1059.

Godsel LM, Dubash AD, Bass-Zubek AE, Amargo EV, Klessner JL, Hobbs RP, Chen X, Green KJ (2010). Plakophilin 2 couples actomyosin remodeling to desmosomal plaque assembly via RhoA. Mol Biol Cell 21, 2844–2859.

Green KJ, Parry DA, Steinert PM, Virata ML, Wagner RM, Angst BD, Nilles LA (1990). Structure of the human desmoplakins. Implications for function in the desmosomal plaque. J Biol Chem 265, 2603–2612.

Green KJ, Simpson CL (2007). Desmosomes: new perspectives on a classic. J Invest Dermatol 127, 2499–2515.

Green KJ, Stappenbeck TS, Parry DA, Virata ML (1992). Structure of desmoplakin and its association with intermediate filaments. J Dermatol 19, 765–769.
Guo Z, Neilson LJ, Zhong H, Murray PS, Zanivan S, Zaidel-Bar R (2014). E-cadherin interactome complexity and robustness resolved by quantitative proteomics. Sci Signal 7, rs7.
Hallock PT, Chin S, Blais S, Neubert TA, Glass DJ (2016). Sorbs1 and -2 Interact with CrkL and Are Required for Acetylcholine Receptor Cluster Formation. Mol Cell Biol 36, 262–227.
Hammerling B, Grund C, Boda-Heggemann J, Moll R, Franke WW (2006). The complexus adhaerens of mammalian lymphatic endothelia revisited: a junction even more complex than hitherto thought. Cell Tissue Res 324, 55–67.
Hatzfeld M (2007). Plakophilins: Multifunctional proteins or just regulators of desmosomal adhesion? Biochim Biophys Acta 1773, 69–77.
He W, Cowin P, Stokes DL (2003). Untangling desmosomal knots with electron tomography. Science 302, 109–113.
Heid HW, Schmidt A, Zimbelmann R, Schafer S, Wintersimanowski S, Stumpp S, Keith M, Figge U, Schnolzer M, Franke WW (1994). Cell-type-specific desmosomal plaque proteins of the plakoglobin family - Plakophilin-1 (band-6 protein). Differentiation 58, 113–131.
Ihrie RA, Marques MR, Nguyen BT, Horner JS, Papazoglu C, Bronson RT, Mills AA, Attardi LD (2005). Perp is a p63-regulated gene essential for epithelial integrity. Cell 120, 843–856.
Iwahara T, Akagi T, Fujitsuka Y, Hanafusa H (2004). CrkII regulates focal adhesion kinase activation by making a complex with Crk-associated substrate, p130Cas. Proc Natl Acad Sci USA 101, 17693–17698.
Johannessen CM, Boehm JS, Kim SY, Thomas SR, Wardwell L, Johnson LA, Emery CM, Stransky N, Cogdill AP, Barretina J, *et al.* (2010). COT drives resistance to RAF inhibition through MAP kinase pathway reactivation. Nature 468, 968-U370.
Kourtidis A, Necela B, Lin WH, Lu R, Feathers RW, Asmann YW, Thompson EA, Anastasiadis PZ (2017). Cadherin complexes recruit mRNAs and RISC to regulate epithelial cell signaling. J Cell Biol 216, 3073–3085.
Kowalczyk AP, Bornslaeger EA, Borgwardt JE, Palka HL, Dhaliwal AS, Corcoran CM, Denning MF, Green KJ (1997). The amino-terminal domain of desmoplakin binds to plakoglobin and clusters desmosomal cadherin-plakoglobin complexes. J Cell Biol 139, 773–784.
Kowalczyk AP, Green KJ (2013). Structure, function, and regulation of desmosomes. Prog Mol Biol Transl Sci 116, 95-118.
Kowalczyk AP, Hatzfeld M, Bornslaeger EA, Kopp DS, Borgwardt JE, Corcoran CM, Settler A, Green KJ (1999). The head domain of plakophilin-1 binds to desmoplakin and enhances its recruitment to desmosomes. Implications for cutaneous disease. J Biol Chem 274, 18145–18148.
Kowalczyk AP, Navarro P, Dejana E, Bornslaeger EA, Green KJ, Kopp DS, Borgwardt JE (1998). VE-cadherin and desmoplakin are assembled into dermal microvascular endothelial intercellular junctions: a pivotal role for plakoglobin in the recruitment of desmoplakin to intercellular junctions. J Cell Sci 111, 3045–3057.
Lamorte L, Royal I, Naujokas M, Park M (2002). Crk adapter proteins promote an epithelial-mesenchymal-like transition and are required for HGF-mediated cell spreading and breakdown of epithelial adherens junctions. Mol Biol Cell 13, 1449–1461.
Lechler T, Fuchs E (2007). Desmoplakin: an unexpected regulator of microtubule organization in the epidermis. J Cell Biol 176, 147–154.
Mandai K, Nakanishi H, Satoh A, Takahashi K, Satoh K, Nishioka H, Mizoguchi A, Takai Y (1999). Ponsin/SH3P12: an l-afadin- and vinculin-binding protein localized at cell-cell and cell-matrix adherens junctions. J Cell Biol 144, 1001–1017.
McGrath JA, McMillan JR, Shemanko CS, Runswick SK, Leigh IM, Lane EB, Garrod DR, Eady RA (1997). Mutations in the plakophilin 1 gene result in ectodermal dysplasia/skin fragility syndrome. Nat Genet 17, 240–244.
McNeil E, Capaldo CT, Macara IG (2006). Zonula occludens-1 function in the assembly of tight junctions in Madin-Darby canine kidney epithelial cells. Molecular Biology of the Cell 17, 1922–1932.
Mueller H, Franke WW (1983). Biochemical and immunological characterization of desmoplakins I and II, the major polypeptides of the desmosomal plaque. J Mol Biol 163, 647–671.
Nekrasova O, Harmon RM, Broussard JA, Koetsier JL, Godsel LM, Fitz GN, Gardel ML, Green KJ (2018). Desmosomal cadherin association with Tctex-1 and cortactin-Arp2/3 drives perijunctional actin polymerization to promote keratinocyte delamination. Nat Commun 9.
Nomme J, Fanning AS, Caffrey M, Lye MF, Anderson JM, Lavie A (2011a). The Src homology 3 domain is required for junctional adhesion molecule binding to the third PDZ domain of the scaffolding protein ZO-1. J Biol Chem 286, 43352–43360.
Nomme J, Fanning AS, Caffrey M, Lye MF, Anderson JM, Lavie A (2011b). The Src homology 3 domain is required for junctional adhesion molecule binding to the third PDZ domain of the scaffolding protein ZO-1. J Biol Chem 286, 43352–43360.
North AJ, Bardsley WG, Hyam J, Bornslaeger EA, Cordingley HC, Trinnaman B, Hatzfeld M, Green KJ, Magee AI, Garrod DR (1999). Molecular map of the desmosomal plaque. J Cell Sci 112 (Pt 23), 4325–4336.
Okada H, Uezu A, Mason FM, Soderblom EJ, Moseley MA 3rd, Soderling SH (2011). SH3 domain-based phototrapping in living cells reveals Rho family GAP signaling complexes. Sci Signal 4, rs13.
O'Neill GM, Fashena SJ, Golemis EA (2000). Integrin signalling: a new Cas(t) of characters enters the stage. Trends Cell Biol 10, 111–119.
Park TJ, Curran T (2008). Crk and Crk-like play essential overlapping roles downstream of disabled-1 in the Reelin pathway. J Neurosci 28, 13551–13562.
Pasdar M, Nelson WJ (1988a). Kinetics of desmosome assembly in Madin-Darby canine kidney epithelial cells: temporal and spatial regulation of desmoplakin organization and stabilization upon cell-cell contact. I. Biochemical analysis. J Cell Biol 106, 677–685.
Pasdar M, Nelson WJ (1988b). Kinetics of desmosome assembly in Madin-Darby canine kidney epithelial cells: temporal and spatial regulation of desmoplakin organization and stabilization upon cell-cell contact. II. Morphological analysis. J Cell Biol 106, 687–695.
Patel DM, Green KJ (2014). Desmosomes in the heart: a review of clinical and mechanistic analyses. Cell Commun Adhes 21, 109–128.
Perez-Moreno M, Davis MA, Wong E, Pasolli HA, Reynolds AB, Fuchs E (2006). p120-catenin mediates inflammatory responses in the skin. Cell 124, 631–644.
Roberts BJ, Johnson KE, McGuinn KP, Saowapa J, Svoboda RA, Mahoney MG, Johnson KR, Wahl JK 3rd (2014). Palmitoylation of plakophilin is required for desmosome assembly. J Cell Sci 127, 3782–3793.
Roberts BJ, Svoboda RA, Overmiller AM, Lewis JD, Kowalczyk AP, Mahoney MG, Johnson KR, Wahl JK 3rd (2016). Palmitoylation of Desmoglein 2 Is a Regulator of Assembly Dynamics and Protein Turnover. J Biol Chem 291, 24857–24865.
Roux KJ, Kim DI, Raida M, Burke B (2012). A promiscuous biotin ligase fusion protein identifies proximal and interacting proteins in mammalian cells. J Cell Biol 196, 801–810.
Ruiz P, Brinkmann V, Ledermann B, Behrend M, Grund C, Thalhammer C, Vogel F, Birchmeier C, Gunthert U, Franke WW, Birchmeier W (1996). Targeted mutation of plakoglobin in mice reveals essential functions of desmosomes in the embryonic heart. J Cell Biol 135, 215–225.
Samuelov L, Sarig O, Harmon RM, Rapaport D, Ishida-Yamamoto A, Isakov O, Koetsier JL, Gat A, Goldberg I, Bergman R, *et al.* (2013). Desmoglein 1 deficiency results in severe dermatitis, multiple allergies and metabolic wasting. Nat Genet 45, 1244–1248.
Schmelz M, Moll R, Kuhn C, Franke WW (1994). Complexus adhaerentes, a new group of desmoplakin-containing junctions in endothelial cells: II. Different types of lymphatic vessels. Differentiation 57, 97–117.
Skerrow CJ, Matoltsy AG (1974). Isolation of epidermal desmosomes. J Cell Biol 63, 515–523.
Stahley SN, Bartle EI, Atkinson CE, Kowalczyk AP, Mattheyses AL (2016). Molecular organization of the desmosome as revealed by direct stochastic optical reconstruction microscopy. J Cell Sci 129, 2897–2904.
Sumigray KD, Chen H, Lechler T (2011). Lis1 is essential for cortical microtubule organization and desmosome stability in the epidermis. J Cell Biol 194, 631–642.
Sumigray KD, Foote HP, Lechler T (2012). Noncentrosomal microtubules and type II myosins potentiate epidermal cell adhesion and barrier formation. J Cell Biol 199, 513–525.
Supek F, Bosnjak M, Skunca N, Smuc T (2011). REVIGO Summarizes and Visualizes Long Lists of Gene Ontology Terms. Plos One 6.
Thomas JW, Ellis B, Boerner RJ, Knight WB, White GC 2nd, Schaller MD (1998). SH2- and SH3-mediated interactions between focal adhesion kinase and Src. J Biol Chem 273, 577–583.
Trinkle-Mulcahy L, Sleeman JE, Lamond AI (2001). Dynamic targeting of protein phosphatase 1 within the nuclei of living mammalian cells. J Cell Sci 114, 4219–4228.
Van Itallie CM, Aponte A, Tietgens AJ, Gucek M, Fredriksson K, Anderson JM (2013). The N and C termini of ZO-1 are surrounded by distinct proteins and functional protein networks. J Biol Chem 288, 13775–13788.
Van Itallie CM, Tietgens AJ, Aponte A, Fredriksson K, Fanning AS, Gucek M, Anderson JM (2014). Biotin ligase tagging identifies proteins proximal to E-cadherin, including lipoma preferred partner, a regulator of epithelial cell-cell and cell-substrate adhesion. J Cell Sci 127, 885–895.

Vasioukhin V, Bowers E, Bauer C, Degenstein L, Fuchs E (2001). Desmoplakin is essential in epidermal sheet formation. Nat Cell Biol 3, 1076–1085.
Vasioukhin V, Degenstein L, Wise B, Fuchs E (1999). The magical touch: genome targeting in epidermal stem cells induced by tamoxifen application to mouse skin. Proc Natl Acad Sci USA 96, 8551–8556.
Woodcock SA, Rooney C, Liontos M, Connolly Y, Zoumpourlis V, Whetton AD, Gorgoulis VG, Malliri A (2009). Src-Induced Disassembly of Adherens Junctions Requires Localized Phosphorylation and Degradation of the Rac Activator Tiam1. Mol Cell 33, 639–653.
Xiao K, Allison DF, Buckley KM, Kottke MD, Vincent PA, Faundez V, Kowalczyk AP (2003a). Cellular levels of p120 catenin function as a set point for cadherin expression levels in microvascular endothelial cells. J Cell Biol 163, 535–545.
Xiao KY, Allison DF, Buckley KM, Kottke MD, Vincent PA, Faundez V, Kowalczyk AP (2003b). Cellular levels of p120 catenin function as a set point for cadherin expression levels in microvascular endothelial cells. J Cell Biol 163, 535–545.
Zandy NL, Playford M, Pendergast AM (2007). Abl tyrosine kinases regulate cell-cell adhesion through Rho GTPases. P Natl Acad Sci USA 104, 17686–17691.